ADVANCED FUNCTIONAL MATERIALS
www.afm-journal.de

A High-Power Symmetric Na-Ion Pseudocapacitor

Zelang Jian, Vadivukarasi Raju, Zhifei Li, Zhenyu Xing, Yong-Sheng Hu, and Xiulei Ji**

Batteries and supercapacitors are critical devices for electrical energy storage with wide applications from portable electronics to transportation and grid. However, rechargeable batteries are typically limited in power density, while supercapacitors suffer low energy density. Here, a novel symmetric Na-ion pseudocapacitor with a power density exceeding 5.4 kW kg^{-1} at 11.7 A g^{-1}, a cycling life retention of 64.5% after 10 000 cycles at 1.17 A g^{-1}, and an energy density of 26 Wh kg^{-1} at 0.585 A g^{-1} is reported. Such a device operates on redox reactions occurring on both electrodes with an identical active material, viz., $Na_3V_2(PO_4)_3$ encapsulated inside nanoporous carbon. This device, in a full-cell scale utilizing highly reversible and high-rate Na-ion intercalational pseudocapacitance, can bridge the performance gap between batteries and supercapacitors. The characteristics of the device and the potentially low-cost production make it attractive for hybrid electric vehicles and low-maintenance energy storage systems.

1. Introduction

The challenge of energy sustainability requires us to move away from fossil fuels towards renewable resources, including solar and wind power.[1] Much attention is focused on the electrical energy storage (EES) systems to store the intermittent renewable energy. The EES solutions also play an important role as dispatchable energy for transportation purposes, including hybrid electric vehicles (HEVs).[2] Essential characteristics of an electric power source for HEVs include high power density and a long cycle/calendar life of more than 10 000 cycles additional to an energy density at least comparable to lead-acid batteries.

Indeed, the core feature needed for HEVs is the high power density. An average power density above ≈10 kW kg^{-1} may allow a typical HEV to be accelerated to a speed of 30 mph by the electric drive alone, thus avoiding operation of the internal combustion engine at its extremely low fuel efficiency.[3] Obviously, this requires high-rate discharge. Moreover, to capture the regenerative braking energy, the device must be recharged very rapidly within a few seconds available during vehicle deceleration. Current HEV electric power sources, including NiMH and Li-ion batteries (LIBs), may provide sufficient power during discharge;[4] however, efficient recharge within a few seconds, e.g., at 500 C to 1000 C (One C is defined as a current rate with a complete charge or discharge sweep in 1 h), represents an almost insurmountable technological barrier for diffusion-controlled redox chemistries.[5] Therefore, capacitive energy storage represents an attractive solution. Capacitive devices are known to have superior cycling life in comparison to batteries. As a matter of fact, supercapacitors have already demonstrated commercial viability in mild HEVs; however, these device modules have low voltages, viz., 25 V, and, as such, are not applicable as a standalone electric drive, since the energy density is too low, viz., ≈8 Wh kg^{-1}.[6]

The "Holy Grail" of capacitive energy storage is to have an energy density up to the level of LIBs and a power density and cycling life identical to supercapacitors.[7] Towards realizing this goal, pseudocapacitors can achieve a much higher energy density than supercapacitors, which would allow their applications as a standalone electric drive and, thus, potentially expanding the HEV market.[8]

For a few decades, efforts have been devoted to pseudocapacitive electrodes that operate on surface or near-surface redox reactions, including RuO_2 hydrates,[9] Co_3O_4,[10] MnO_2,[11] $Ni(OH)_2$,[12] and $NiCoO_2$.[13] A common feature of these electrodes is that they operate in aqueous electrolytes by using protons for charge compensation, which limits the full-cell voltage below 1.5 V with a limited energy density. In order to increase the energy density, recently, pseudocapacitive chemistry has been explored in non-aqueous electrolytes, where Li or Na ions are used for charge compensation.

Recently, Dunn and co-workers reported Li-ion intercalational pseudocapactive behavior of nanosized TiO_2,[14] MoO_3,[15] and Nb_2O_5[16] in nonaqueous electrolytes. To date, most studies investigate intercalational pseudocapacitance in half cells with Li or Na metal as a counter electrode, while full cell configurations have been rarely studied. For a full cell design, ideally, both electrodes should exhibit intercalational pseudocapacitance, and the cathode compositions should comprise removable Li or Na ions so that these ions can be de-intercalated and intercalated into the anode during the first charge of the cell.[17] One significant benefit of such systems is that the cell

Dr. Z. Jian, Dr. V. Raju, Z. Li, Z. Xing, Prof. X. Ji
Department of Chemistry
Oregon State University
Corvallis, OR 97331-4003, USA
E-mail: david.ji@oregonstate.edu
Prof. Y.-S. Hu
Key Laboratory for Renewable Energy
Beijing Key Laboratory for New Energy Materials and Devices
Beijing National Laboratory for Condensed Matter Physics
Institute of Physics
Chinese Academy of Sciences
Beijing 100190, China
E-mail: yshu@aphy.iphy.ac.cn

DOI: 10.1002/adfm.201502433

operation does not require much electrolyte usage, which is exactly the challenge of the hybrid metal-ion capacitors. Hybrid metal-ion capacitors have activated carbon (AC) as the positive electrode and graphitic carbon or $Li_4Ti_5O_{12}$ as the negative electrode but the transport ions cannot be supplied by either electrode, which limits the energy density of the full cell.[18] Na-ion batteries (NIBs) have attracted much attention due to the low cost and wide distribution of sodium resource.[19] Among different NIBs electrodes, $Na_3V_2(PO_4)_3$ with the NASICON structure exhibits high Na-ion diffusion coefficient, and shows both cathodic and anodic electrochemical properties.[20–22] Two Na ions can be extracted from or one Na ion can be inserted into the $Na_3V_2(PO_4)_3$ host, thus exhibiting two distinctive plateaus of 3.4 and 1.6 V vs. Na^+/Na with a theoretical capacity of 118 and 59 mAh g^{-1}, respectively.[20,21,23] The symmetric battery using $Na_3V_2(PO_4)_3$ as both cathode and anode with a cell operating voltage of ≈1.8 V was reported with promising rate capability of full devices. However, only limited cycling performance was demonstrated with relatively poor power performance.[24,25] Duan et al. demonstrated the capacity retention of 81.4% after 50 cycles in the voltage window of 1.0–2.2 V.[24] Li et al. reported the capacity retention of 80% after 200 cycles in 1.0–3.0 V.[25]

Here, we transform this chemistry of NIB into a Na-ion pseudocapacitor by comprehensively improving its rate capability. We report the full-cell Na-ion intercalational pseudocapacitor, which operates on oxidation/reduction reactions occurring on both electrodes with an identical active material, viz., $Na_3V_2(PO_4)_3$ encapsulated inside nanoporous carbon. This device, utilizing highly reversible, high-rate, cost-effective Na-ion intercalational pseudocapacitance, can bridge the performance gap between batteries and supercapacitors.

2. Results

In order to turn $Na_3V_2(PO_4)_3$ "capacitive," its conductivity, both ionic and electronic, of the electrodes needs to be optimized. The ion transport in a solid follows the equation:[26]

$$t = L^2/2D \quad (1)$$

where t is the mean diffusion time; D is determined by diffusivity, and L is the diffusion length. In order to reduce charge/discharge time, we choose to shorten the ion migration length by nanosizing the active mass. On the other hand, $Na_3V_2(PO_4)_3$ is an electronic insulator as NASICON is, indeed, a solid-state electrolyte similar with its lithium counterpart.[27] In addressing this issue, we increase the electronic conductivity by generating $Na_3V_2(PO_4)_3$ nanoparticles inside a nanoporous carbon framework that serves as an electronic conduit. Furthermore, the nanoporosity inside the carbon/$Na_3V_2(PO_4)_3$ nanocomposite provides extensive contact sites between $Na_3V_2(PO_4)_3$ and imbibed liquid electrolyte.

The challenge is how to infiltrate $Na_3V_2(PO_4)_3$, a quaternary compound, into a nanoporous carbon. We have overcome this challenge with a two-step infiltration. First, we infiltrated V_2O_5 nanoparticles into nanoporous carbon by our established ambient hydrolysis deposition (AHD) method.[28,29] Then, we reacted the C/V_2O_5 nanocomposite with infiltrated NaH_2PO_4 to form C/$Na_3V_2(PO_4)_3$, referred to as NVP–AHD.

The preparation of C/V_2O_5 nanocomposite with 20 wt% of V_2O_5 is described in our previous work.[28] To prepare NVP–AHD, the as-prepared C/V_2O_5 nanocomposite was soaked in an ethanol–water solution with the stoichiometric amount of NaH_2PO_4. After the solvent was evaporated, the solid mixture was calcined at 700 °C for 10 h, forming the black powder of NVP–AHD. For comparison, bulk $Na_3V_2(PO_4)_3$, referred to bulk-NVP was also prepared by the reported solid-state reaction.[20] More details are provided in Experimental Section.

Powder XRD patterns of the NVP–AHD and bulk-NVP samples reveal the pure phase with all the peaks indexed to $Na_3V_2(PO_4)_3$ (**Figure 1**a). This confirms that carbothermal reaction does occur during the solid-state annealing, which may reduce V (5+) in V_2O_5 to V (3+) in $Na_3V_2(PO_4)_3$. Bulk-NVP displays sharp peaks while NVP–AHD shows much broadened peaks. The $Na_3V_2(PO_4)_3$ domain sizes in NVP–AHD are calculated, based on different diffraction peaks, to be around 14 nm according to the Scherrer equation.

Transmission electron microscopy (TEM) and high-angle angular dark-filed scanning TEM (HAADF-STEM) confirm the small particle sizes of $Na_3V_2(PO_4)_3$ in NVP–AHD to be less than 20 nm, in good agreement with the XRD results, as shown in **Figure 2**a,b. The fine distribution of the NVP nanoparticles in NVP–AHD is revealed by the energy-dispersive X-ray (EDX) mapping of C, Na, and P elements with the nearly identical shape of maps, as shown in Figure 2c. In sharp contrast, bulk

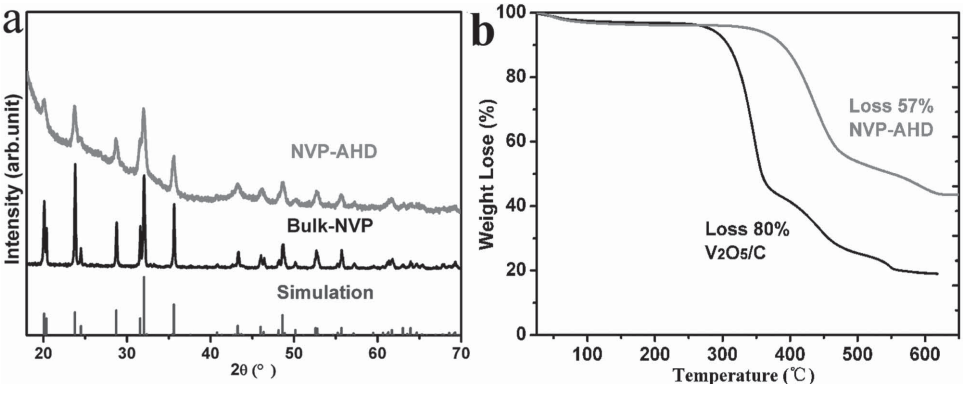

Figure 1. a) XRD patterns of the NVP–AHD and bulk-NVP samples. b) TG curves of the NVP–AHD and V_2O_5/C samples in air atmosphere.

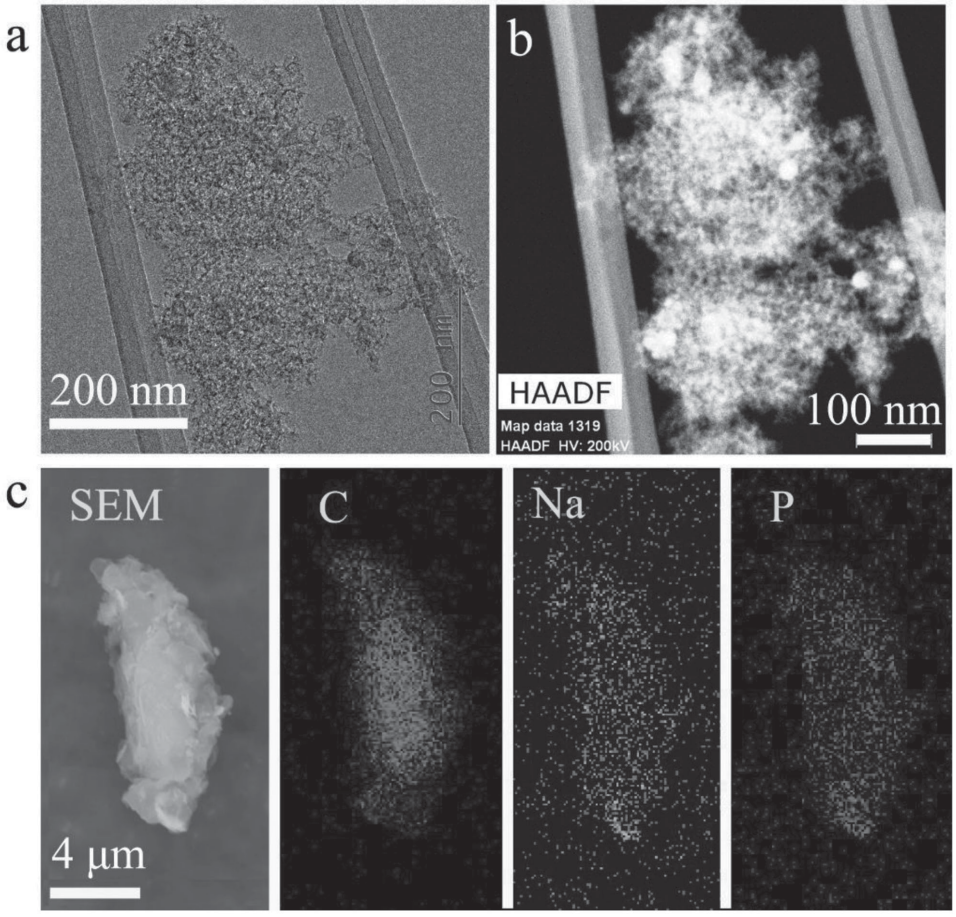

Figure 2. a) TEM image and b) HAADF-STEM image of the NVP–AHD sample. c) SEM image and EDX maps (of the C, Na, and P elements) of the NVP–AHD sample.

$Na_3V_2(PO_4)_3$ exhibits large particle size of ≈10 μm, as shown in the SEM image of the physical mixture of bulk-NVP and nanoporous carbon (Figure S1, Supporting Information).

Thermogravimetric analysis (TGA) shows that there is ca. 40 wt% of $Na_3V_2(PO_4)_3$ in the NVP–AHD (considering the oxidation of V(3+)), which is slightly more than the theoretical value of 38.5 wt% based on the amount of V_2O_5 in C/V_2O_5. Figure 1b shows the TGA curves of NVP–AHD and C/V_2O_5 samples under an oxygen atmosphere. Interestingly, the onset temperatures for carbon oxidation are vastly different for these two samples: 380 °C for NVP–AHD and 300 °C C/V_2O_5, further confirming a complete conversion of V_2O_5 to $Na_3V_2(PO_4)_3$.

After $Na_3V_2(PO_4)_3$ generation, the surface area of the pure nanoporous carbon decreased from 984 to 458 m^2 g^{-1}. **Figure 3**a,b show the N_2 sorption isotherms and pore size distribution (PSD) of the nanoporous carbon and NVP–AHD samples. The PSD of the nanoporous carbon is around 40 nm, while after $Na_3V_2(PO_4)_3$ infiltration the composite exhibits a bimodal nanoporous structure with pore sizes centered around 40 and 20 nm, respectively. This suggests that $Na_3V_2(PO_4)_3$ nanoparticles do nucleate in the nanopores of mesoporous carbon and its particle size is less than 20 nm, which is in good agreement with the XRD and TEM results.

The above results collectively reveal that we have successfully infiltrated $Na_3V_2(PO_4)_3$ nanoparticles with a fine dispersion inside nanoporous carbon in NVP–AHD.

Na ions can be either extracted from or inserted into $Na_3V_2(PO_4)_3$, which enables NVP–AHD as both cathode and anode.[20,24,25] We investigated both the cathodic and anodic behaviors of NVP–AHD, with NVP–AHD as the working electrode and sodium foil as the counter/reference electrode. **Figure 4**a,b show the galvanostatic charge–discharge profiles for the first three cycles at 1C (1C is defined as 117 mA g^{-1}) in the cathode and anode voltage ranges, respectively. As the cathode, NVP–AHD exhibits a plateau at 3.3 V vs. Na^+/Na and two slopes before and after the plateau. The discharge capacity based on the whole composite mass is 53 mAh g^{-1}. As the anode, NVP–AHD shows one plateau at 1.6 V vs. Na^+/Na and two slopes before and after the plateau as well, whose capacity is 38 mAh g^{-1}. Importantly, as cathode and anode, NVP–AHD displays high initial Coulombic efficiency of 85% and 88%, respectively, which promises a great potential for a full cell device. We also tested the Na-ion storage capacity for the pure nanoporous carbon in the above voltage range, which gives rise to 18 mAh g^{-1} for the cathode and 31 mAh g^{-1} for the anode (as shown in Figure S2 and Figure S3, Supporting Information). This explains the higher capacity contribution from the slopes

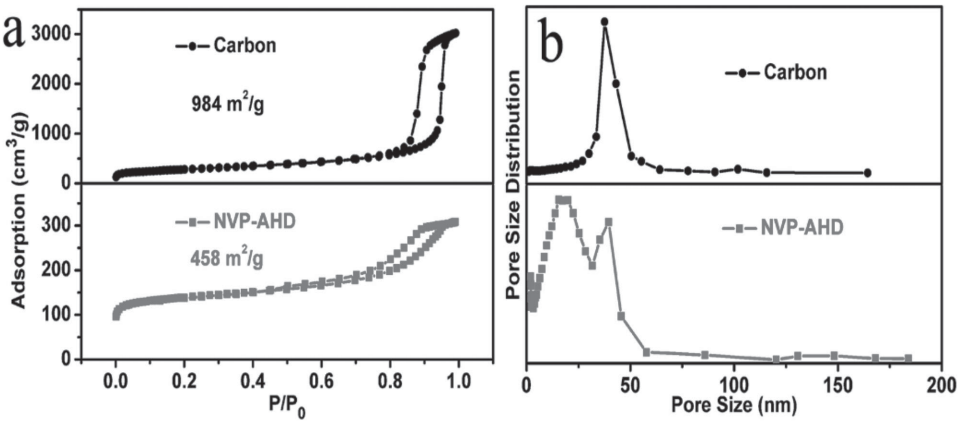

Figure 3. a) Nitrogen adsorption–desorption isotherms and b) pore size distribution of the as-prepared nanoporous carbon and NVP–AHD samples.

when NVP–AHD is an anode. By taking out the capacity contribution from the porous carbon, the $Na_3V_2(PO_4)_3$ phase exhibits impressive capacities of 106 and 49 mAh g^{-1} for the cathode and anode, respectively. Considering the nanoporous carbon in the composite is of a lower surface area compared to the pure nanoporous carbon, the capacity contribution from the carbon component in the composite is overestimated. Therefore, the specific capacity of the NVP should have been underestimated. Thus, it is evident that NVP approaches its theoretical capacity on both anodic and cathodic sides.

We further investigated the performance of full cells with NVP–AHD as both cathode and anode. We set the mass ratio between cathode and anode as 2:3 to match their capacities. Full cells with bulk-NVP as electrodes are also assembled for comparison purposes, where the active mass consists of a physical mixture of 60 wt% nanoporous carbon and 40 wt% bulk-NVP. Cyclic voltammetry (CV) measurements are conducted for the full cells at di erent scanning rates between 0.2 and 2.7 V (**Figure 5**a,b). Compared with bulk-NVP, NVP–AHD displays higher specific capacity in CV curves and smaller potential gaps between the corresponding anodic and cathodic peaks. A wider gap means a higher overpotential and more sluggish reactions. The potential gaps for the NVP–AHD cell are of 0.20, 0.31, and 0.43 V compared with 0.45, 0.64, and 0.79 V for the bulk-NVP cell at low scan rates of 2, 5, and 10 mV s^{-1}, respectively. At high scan rates, NVP–AHD still exhibits redox peaks in its CV curves, while redox peaks from bulk-NVP significantly attenuate. Furthermore, NVP–AHD exhibits much higher capacity than bulk-NVP, as shown in Figure 5c,d. NVP–AHD still displays redox peaks in the profiles at high currents, which is due to the short Na-ion diffusion distance in NVP nanoparticles. Such redox peaks are not observed at high currents from bulk-AHD, which shows pure capacitive behavior of the nanoporous carbon in the mixture. **Figure 6**a shows the corresponding energy densities at different current rates, where NVP–AHD is much superior to bulk-NVP. NVP–AHD full cell delivers an energy density of 26 Wh kg^{-1} at 0.585 A g^{-1} and 15 Wh kg^{-1} at a high current of 11.7 A g^{-1} (specific energy is calculated based on the discharge energy output and the total mass of both electrodes). Note that at 11.7 A g^{-1}, it takes only 7 s to complete the charge or discharge of the cell, corresponding an average specific power of 5424 W kg^{-1}, as shown in Figure 6b. NVP symmetrical batteries were reported with less than 200 cycles in previous works.[24,25] In contrast, the full cell of NVP–AHD presents an unprecedented excellent cycling performance with 83% of energy density after 4000 deep cycles (cell discharged to 0.2 V) at a current density of 1.17 A g^{-1} (10 C), as shown in Figure 6c. Even after 10,000 deep cycles, the energy density still retains 64.5%.

We attribute the excellent Na-ion storage performance to the unique nanostructure of NVP–AHD: 1) NVP with 3D network structure facilitates fast ionic diffusion; 2) Small particle size

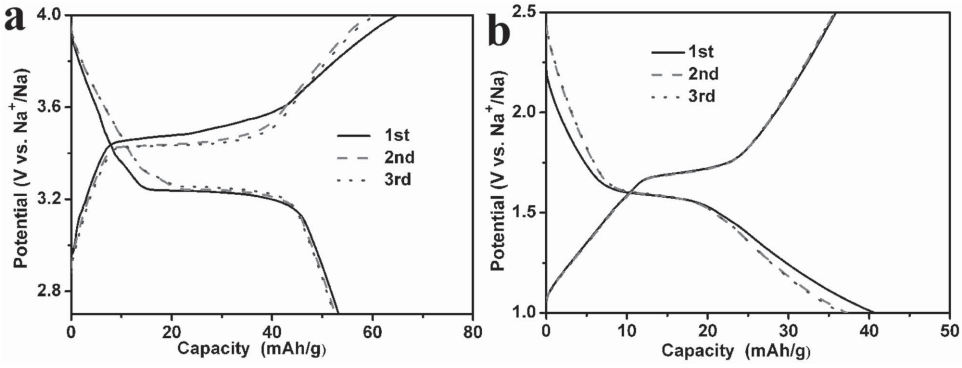

Figure 4. First-three sodiation/desodiation profiles at 1C current rate of the NVP–AHD sample as a) cathode and b) anode.

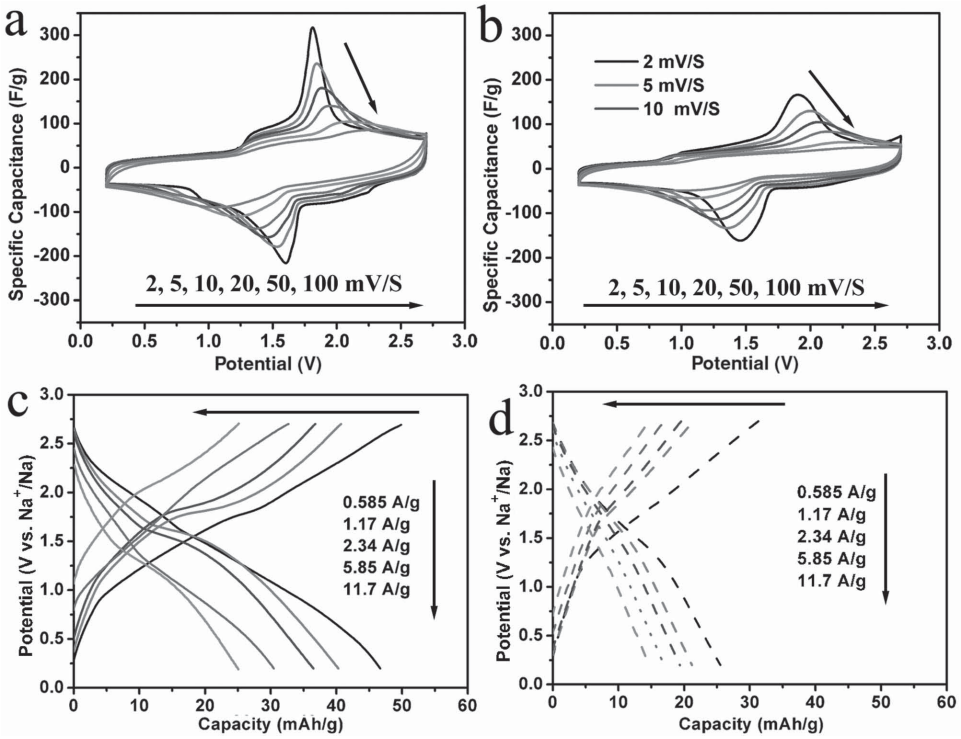

Figure 5. CV curves at different scanning rates for the a) NVP–AHD and b) bulk-NVP with nanoporous carbon mixture; sodiation/desodiation profiles of the c) NVP–AHD and d) bulk-NVP with nanoporous carbon mixture.

shortens the Na-ion diffusion length; 3) Nanoporous carbon provides an effective electronic conductivity; 4) The porous structure provides the maximized electrolyte/active mass contacts.

3. Discussion

We further investigated the charge-storage mechanism in the NVP–AHD, which can be classified into the diffusion-controlled Faradaic reaction and the capacitive behavior. The latter include intercalational pseudocapacitance and the non-Faradaic electrical double-layer (EDL) capacitance. We analyzed the relationship between the peak currents and the CV scan rates for the NVP–AHD cell, as shown in **Figure 7**a,b. A linear relationship is found to be well fitted between the peak currents and square root of the low scan rates (<10 mV s^{-1}), indicating a diffusion-controlled reversible process. The linear relationship between the peak currents and the high scan rates (>10 mV s^{-1}) is well fitted, indicating capacitive behavior. The results are good agreement with previous work.[15]

Based on the above analysis, NVP–AHD sample displays better electrochemical performance, where the composite with tiny particles is expected to exhibit significant pseudocapacitance.[28,30] We employ the following equation:

$$i(V) = k_1 v + k_2 v^{1/2} \quad (2)$$

where, $k_1 v$ represents the total capacitive contribution while $k_2 v^{1/2}$ stands for the contribution of diffusion-controlled Faradaic intercalation process. The fitting results, as shown in **Figure 8**a, (for more details, please see our previous work[28]) show that the capacitive contribution in the NVP–AHD sample is 64% at the scan rate of 5 mV s^{-1}.

We expect to further distinguish our device from other pseudocapacitors in terms of electrolyte usage. We assembled a NVP–AHD symmetric full cell with no Na ions in the electrolyte by using 1.0 M tetraethylammonium (TEA^+) tetrafluoroborate (BF_4^-) in ethylene carbonate–dimethyl carbonate (EC–DMC, 1:1, v/v) as the electrolyte. With such an electrolyte, we achieve 73% of the original capacity (see the Figure 8b). This is because the NVP–AHD as cathode can supply Na ions, leading to high charge storage retention rate and less electrolyte dosage.

4. Conclusion

In summary, we synthesized a nanocomposite that contains a quaternary compound—$Na_3V_2(PO_4)_3$ in a nanoporous carbon (NVP–AHD) by the AHD method. In this novel nanocomposite, a synergistic electronic/ionic conducting network is formed, leading to an excellent electrochemical performance. Furthermore, such a device operates on redox reactions occurring on both electrodes of the identical composition, viz., $Na_3V_2(PO_4)_3$ encapsulated inside nanoporous carbon. This device, for the first time, utilizes highly reversible, high-rate, and cost-effective Na-ion intercalational pseudocapacitance for both identical electrodes in a non-aqueous electrolyte. Its energy density reaches 26 Wh kg^{-1}, meeting the target of capacitor. Even at a

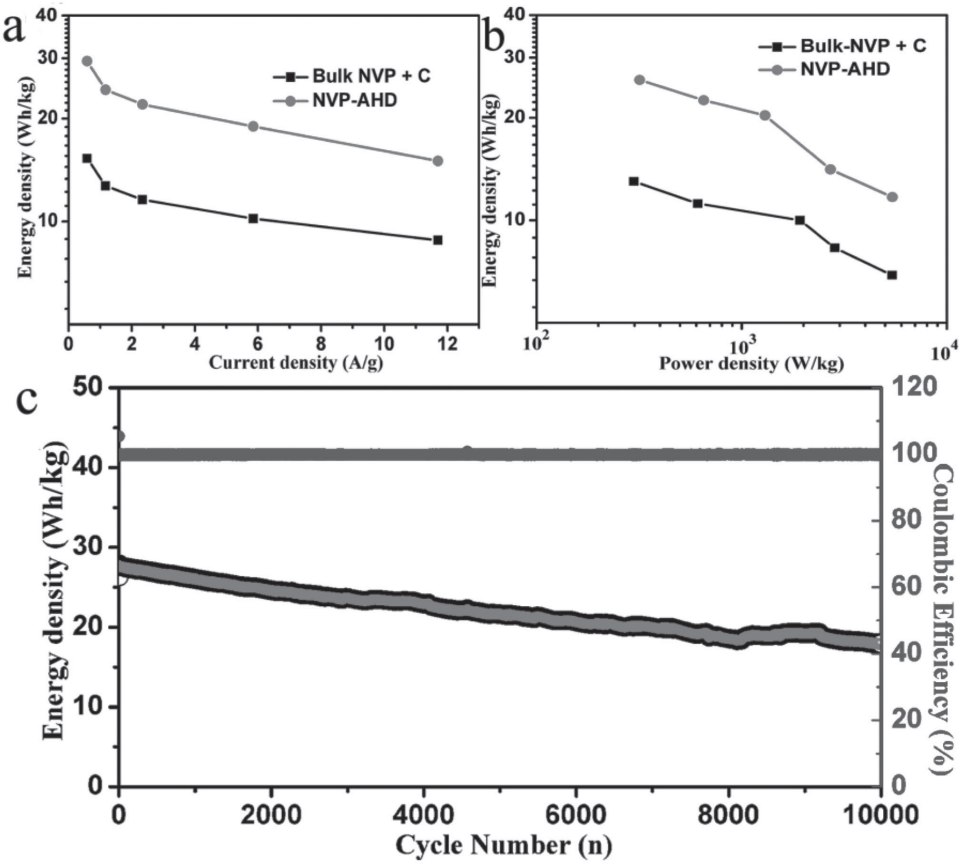

Figure 6. a) Energy density of NVP–AHD and bulk-NVP with nanopores carbon mixture in symmetric Na-ion pseudocapacitors. b) Ragone plots of the NVP–AHD and bulk-NVP with nanopores carbon mixture in symmetric Na-ion pseudocapacitors. c) Long-cycling performance of the NVP–AHD symmetric Na-ion pseudocapacitors.

high current of 11.7 A g^{-1}, its energy density is 15 Wh kg^{-1}; in this case, its power density reaches 5424 W kg^{-1}. After 10 000 cycles at 1.17 A g^{-1}, the energy density retains its 64.5%. Charge-storage mechanism study reveals that diffusion-controlled reversible process dominates at low scan rates and capacitive behavior plays the primary role at high scan rates. Symmetric pseudocapacitors with the same material as both negative and positive electrodes may substantially decrease the materials' processing cost and reduce complexity as well as enhance manufacturability of such devices, which can serve as an electric power source for full HEVs and low-maintenance energy storage system.

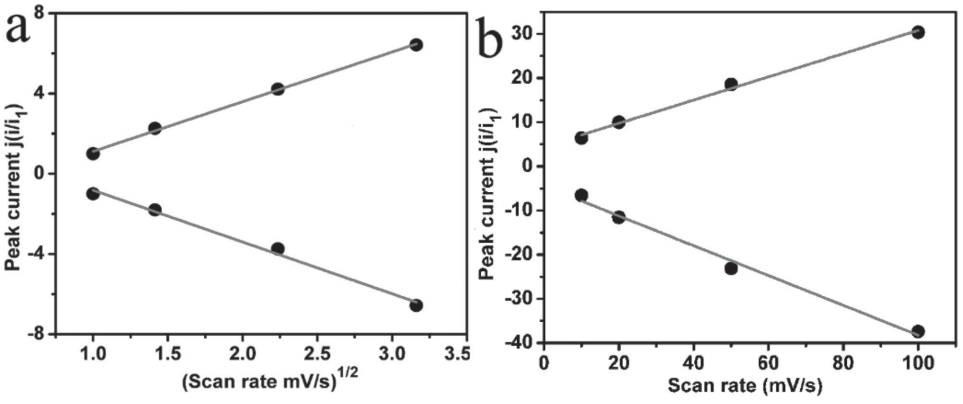

Figure 7. Relationship between the square root of scan rates (≤10 mV s^{-1}) (a) or scan rates (≥10 mV s^{-1}) (b) and normalized peak current, i/i_1, where i_1 is the peak current at the scan rate of 1 mV s^{-1} and i is peak current at different scan rates. The point plots are experimental values, and the lines are fitting results.

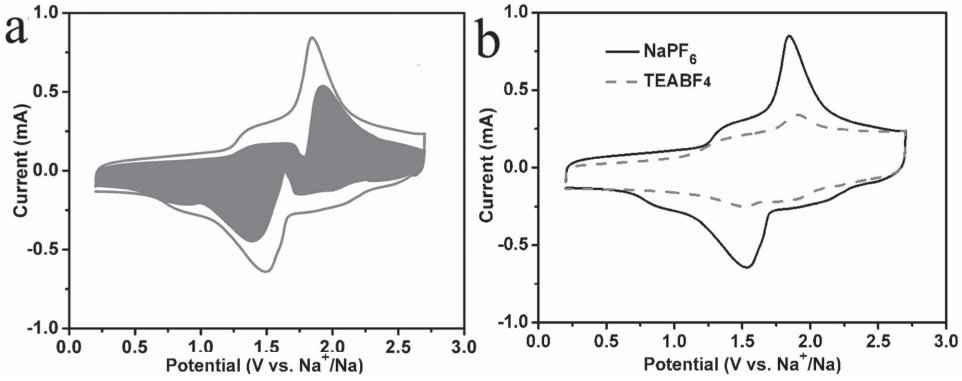

Figure 8. a) CV profile of NVP–AHD at a scan rate of 5 mV s^{-1}. The estimated capacitive current contribution is shown in the shaded region. b) Comparison of CV curves of NVP–AHD with 1.0 M $NaPF_6$ and 1.0 M $TEABF_4$ in EC–DMC (1:1, v/v) at a scan rate of 5 mV s^{-1}.

5. Experimental Section

First, nanoporous carbon with uniform porosity was obtained by using a template method, as described in ref. [31] in which resorcinol and formaldehyde are precursors for polymerization around the Ludox nanospheres. Then, the obtained nanoporous carbon (150 mg) was allowed to equilibrate in an atmospheric water vapor/air mixture with 100% relative pressure at 80 °C for 1 h. After aging for 1 h at ambient conditions, water-loaded nanoporous carbon was dispersed and soaked for 1 h in a dilute solution of vanadium triisopropoxide solvated in cyclohexane (10 vol%). The solid product was collected by filtration in a glovebox. C/V_2O_5 nanocomposite was obtained after being heated at 225 °C in air for 2 h. Finally, the as-prepared C/V_2O_5 was soaked with the stoichiometric amount of NaH_2PO_4 ethanol–water solution. After the solvent was evaporated, the solid mixture was calcined at 700 °C for 10 h, forming the black powder of NVP–AHD. For comparison, bulk $Na_3V_2(PO_4)_3$, was also prepared as reported solid-state reaction and mixed with nanoporous carbon physically, which is referred to as bulk-NVP.[20]

Powder X-ray diffraction (XRD) was performed to characterize the NVP–AHD and bulk-NVP on a Rigaku Ultima IV Diffractometer with Cu K α (λ = 1.5406 Å) radiation. TG curve of the V_2O_5@C and NVP–AHD samples was obtained using a Shimadzu TGA-50 instrument in air from room temperature to 800 °C with a ramping rate of 10 °C min^{-1}. The specific surface area was calculated by the Brunauer-Emmett-Teller (BET) method using the adsorption branch. The morphology is examined by an FEI NOVA 230 high-resolution scanning electron microscopy (SEM) and FEI Titan 80-200 TEM coupled with a high-angle annular dark-field (HAADF) detector.

The electrodes were prepared with active materials, carbon additive, and polytetrafluoroethylene (PTFE) at a weight ratio of 80:10:10. The slurry was cast on pure Al mesh and dried at 100 °C in vacuum for 10 h. The coin cells CR2032 were assembled with pure sodium foil as counter electrode, a glass fiber as separator, and 1 M $NaPF_6$ EC:DMC (1:1) as electrolyte in an argon-filled glove box. The electrochemical measurements were performed on Arbin BT2000 system at room temperature. The Na storage tests of NVP–AHD or bulk-NVP with nanoporous carbon as cathode and anode were performed at a voltage range of 2.7–4.0 and 1.0–2.5 V vs. Na^+/Na, respectively. The symmetric pseudocapacitor device was constructed using NVP–AHD or bulk-NVP with nanoporous carbon as both the cathode and anode electrodes in a 2032 coin-type cell. The symmetric pseudocapacitor device was sodiated and desodiated between the voltage range of 0.2–2.7 V at different currents. The capacity was calculated based on the both cathode and anode mass. The energy density was divided the discharge energy by the total mass of cathode and anode. CV was performed on a Bio-Logic VMP3.

Supporting Information

Supporting Information is available from the Wiley Online Library or from the author.

Acknowledgements

X.J. gratefully acknowledges the financial support from Advanced Research Projects Agency-Energy (ARPA-E), Department of Energy of the United States, Award number: DE-AR0000297TDD. Y.-S.H. acknowledges the support from NSFC (51222210 and 11234013, China).

Received: June 15, 2015
Revised: July 21, 2015
Published online: August 13, 2015

[1] a) M. Armand, J.-M. Tarascon, *Nature* **2008**, *451*, 652; b) M. Winter, R. J. Brodd, *Chem. Rev.* **2004**, *104*, 4245; c) M. Dresselhaus, I. Thomas, *Nature* **2001**, *414*, 332.
[2] a) M. M. Thackeray, C. Wolverton, E. D. Isaacs, *Energy Environ. Sci.* **2012**, *5*, 7854; b) D. Deng, M. G. Kim, J. Y. Lee, J. Cho, *Energy Environ. Sci.* **2009**, *2*, 818; c) C. D. Wessells, S. V. Peddada, R. A. Huggins, Y. Cui, *Nano Lett.* **2011**, *11*, 5421.
[3] a) P. Simon, Y. Gogotsi, *Nat. Mater.* **2008**, *7*, 845; b) Y. Zhu, S. Murali, M. D. Stoller, K. Ganesh, W. Cai, P. J. Ferreira, A. Pirkle, R. M. Wallace, K. A. Cychosz, M. Thommes, *Science* **2011**, *332*, 1537.
[4] a) B. Scrosati, J. Hassoun, Y.-K. Sun, *Energy Environ. Sci.* **2011**, *4*, 3287; b) L.-F. Cui, Y. Yang, C.-M. Hsu, Y. Cui, *Nano Lett.* **2009**, *9*, 3370.
[5] a) Z. Yu, B. Duong, D. Abbitt, J. Thomas, *Adv. Mater.* **2013**, *25*, 3302; b) Y. Huang, J. Liang, Y. Chen, *Small* **2012**, *8*, 1805.
[6] a) A. Chu, P. Braatz, *J. Power Sources* **2002**, *112*, 236; b) M. Mastragostino, F. Soavi, *J. Power Sources* **2007**, *174*, 89; c) Z. Xing, B. Wang, W. Gao, C. Pan, J. K. Halsted, E. S. Chong, J. Lu, X. Wang, W. Luo, C.-H. Chang, *Nano Energy* **2015**, *11*, 600.
[7] N. S. Choi, Z. Chen, S. A. Freunberger, X. Ji, Y. K. Sun, K. Amine, G. Yushin, L. F. Nazar, J. Cho, P. G. Bruce, *Angew. Chem. Int. Ed.* **2012**, *51*, 9994.
[8] a) H. Wang, H. S. Casalongue, Y. Liang, H. Dai, *J. Am. Chem. Soc.* **2010**, *132*, 7472; b) L. Yang, S. Cheng, Y. Ding, X. Zhu, Z. L. Wang, M. Liu, *Nano Lett.* **2011**, *12*, 321.

[9] C.-C. Hu, K.-H. Chang, M.-C. Lin, Y.-T. Wu, *Nano Lett.* **2006**, *6*, 2690.
[10] J. Liu, J. Jiang, C. Cheng, H. Li, J. Zhang, H. Gong, H. J. Fan, *Adv. Mater.* **2011**, *23*, 2076.
[11] X. Lang, A. Hirata, T. Fujita, M. Chen, *Nat. Nanotechnol.* **2011**, *6*, 232.
[12] H. Li, M. Yu, F. Wang, P. Liu, Y. Liang, J. Xiao, C. Wang, Y. Tong, G. Yang, *Nat. Commun.* **2013**, *4*, 1894.
[13] G. Zhang, X. W. D. Lou, *Adv. Mater.* **2013**, *25*, 976.
[14] a) J. Wang, J. Polleux, J. Lim, B. Dunn, *J. Phys. Chem. C* **2007**, *111*, 14925; b) T. Brezesinski, J. Wang, J. Polleux, B. Dunn, S. H. Tolbert, *J. Am. Chem. Soc.* **2009**, *131*, 1802.
[15] T. Brezesinski, J. Wang, S. H. Tolbert, B. Dunn, *Nat. Mater.* **2010**, *9*, 146.
[16] V. Augustyn, J. Come, M. A. Lowe, J. W. Kim, P.-L. Taberna, S. H. Tolbert, H. D. Abruña, P. Simon, B. Dunn, *Nat. Mater.* **2013**, *12*, 518.
[17] X. Wang, S. Kajiyama, H. Iinuma, E. Hosono, S. Oro, I. Moriguchi, M. Okubo, A. Yamada, *Nat. Commun.* **2015**, *6*, 1138.
[18] a) K. Naoi, S. Ishimoto, Y. Isobe, S. Aoyagi, *J. Power Sources* **2010**, *195*, 6250; b) J. Ding, H. Wang, Z. Li, K. Cui, D. Karpuzov, X. Tan, A. Kohandehghan, D. Mitlin, *Energy Environ. Sci.* **2015**, *8*, 941; c) V. Aravindan, W. Chuiling, S. Madhavi, *J. Mater. Chem.* **2012**, *22*, 16026; d) Y.-G. Wang, Y.-Y. Xia, *Electrochem. Commun.* **2005**, *7*, 1138.
[19] a) S. W. Kim, D. H. Seo, X. Ma, G. Ceder, K. Kang, *Adv. Energy Mater.* **2012**, *2*, 710; b) M. D. Slater, D. Kim, E. Lee, C. S. Johnson, *Adv. Funct. Mater.* **2013**, *23*, 947; c) H. Pan, Y.-S. Hu, L. Chen, *Energy Environ. Sci.* **2013**, *6*, 2338; d) N. Yabuuchi, K. Kubota, M. Dahbi, S. Komaba, *Chem. Rev.* **2014**, *114*, 11636; e) C. Bommier, X. Ji, *Isr. J. Chem.* **2015**, *55*, 486.
[20] Z. Jian, L. Zhao, H. Pan, Y.-S. Hu, H. Li, W. Chen, L. Chen, *Electrochem. Commun.* **2012**, *14*, 86.
[21] Z. Jian, W. Han, Y. Liang, Y. Lan, Z. Fang, Y.-S. Hu, Y. Yao, *J. Mater. Chem. A* **2014**, *2*, 20231.
[22] Z. Jian, Y. Sun, X. Ji, *Chem. Commun.* **2015**, *51*, 6381.
[23] a) Z. Jian, W. Han, X. Lu, H. Yang, Y. S. Hu, J. Zhou, Z. Zhou, J. Li, W. Chen, D. Chen, *Adv. Energy Mater.* **2013**, *3*, 156; b) Z. Jian, C. Yuan, W. Han, X. Lu, L. Gu, X. Xi, Y. S. Hu, H. Li, W. Chen, D. Chen, *Adv. Funct. Mater.* **2014**, *24*, 4265; c) Q. An, F. Xiong, Q. Wei, J. Sheng, L. He, D. Ma, Y. Yao, L. Mai, *Adv. Energy Mater.* **2015**, *5*, 1401963.
[24] W. Duan, Z. Zhu, H. Li, Z. Hu, K. Zhang, F. Cheng, J. Chen, *J. Mater. Chem. A* **2014**, *2*, 8668.
[25] S. Li, Y. Dong, L. Xu, X. Xu, L. He, L. Mai, *Adv. Mater.* **2014**, *26*, 3545.
[26] a) G. Wang, D. Bradhurst, S. Dou, H. Liu, *J. Power Sources* **2003**, *124*, 231; b) W.-J. Cui, Y. JIN, L. Chen, C.-X. Wang, Y.-Y. Xia, *J. Power Sources* **2012**, *217*, 77; c) Y. G. Guo, J. S. Hu, L. J. Wan, *Adv. Mater.* **2008**, *20*, 2878.
[27] Q. Wei, Q. An, D. Chen, L. Mai, S. Chen, Y. Zhao, K. M. Hercule, L. Xu, A. Minhas-Khan, Q. Zhang, *Nano Lett.* **2014**, *14*, 1042.
[28] V. Raju, J. Rains, C. Gates, W. Luo, X. Wang, W. F. Stickle, G. D. Stucky, X. Ji, *Nano Lett.* **2014**, *14*, 4119.
[29] X. Wang, V. Raju, W. Luo, B. Wang, W. F. Stickle, X. Ji, *J. Mater. Chem. A* **2014**, *2*, 2901.
[30] G. Yu, L. Hu, M. Vosgueritchian, H. Wang, X. Xie, J. R. McDonough, X. Cui, Y. Cui, Z. Bao, *Nano Lett.* **2011**, *11*, 2905.
[31] S. Han, T. Hyeon, *Chem. Commun.* **1999**, 1955.